Research Paper
J. Astron. Space Sci. 39(3), 99-108 (2022)
https://doi.org/10.5140/JASS.2022.39.3.99

JASS Journal of Astronomy and Space Sciences

On the Influence of the Moment of Inertia of Gas on the Galactic Rotation Curves

Yuriy A. Portnov†
Moscow Automobile and Road Construction State Technical University (MADI), Moscow 125319, Russia

There are two models that explain the rotation curves of galaxies: dark matter, which gives the missing contribution to the gravitational potential of the standard theory of gravity, and modified theories of gravity, according to which the gravitational potential is created by ordinary visible mass. Both models have some disadvantages. The article offers a new look at the problem of galactic rotation curves. The author suggests that the moment of inertia creates an additional gravitational potential along with the mass. The numerical simulation carried out on the example of fourteen galaxies confirms the validity of such an assumption. This approach makes it possible to explain the constancy of gas velocities outside the galactic disk without involving the hypothesis of the existence of dark matter. At the same time, the proposed approach lacks the disadvantages of modified theories of gravity, where the gravitational potential is created only by the mass of visible matter.

Keywords: moment of inertia, dark matter, modified theory of gravity, galactic rotation curves, gas in galaxies

1. INTRODUCTION

When it was discovered that the rotational dynamics of stars and gas on the outskirts of the galaxy did not correspond to the mass of the visible matter of the galaxy, two hypotheses were put forward to explain this phenomenon: the hypothesis of the existence of dark matter and the hypothesis of the need to modify the theory of gravity [for example, modified Newtonian dynamics (MoND) and tensor-vector-scalar theory of gravity (TeVeS)]. Such a choice of hypotheses was not accidental, as it proved itself well in the study of the solar system. Thus, to explain the anomalies in the motion of Uranus, a hypothesis was put forward about the existence of another unknown and, at the time, unobservable planet of the solar system Neptune. Later, another planet of the solar system, Pluto, was discovered by the same method. The precession of Mercury's orbit could not be explained by the additional planet Vulcan, but it was explained by the transition from Newton's theory of gravity to the general theory of relativity. In this regard, the hypotheses put forward to explain anomalies in the motion of stars and gas outside galaxies seem to be logical, but both of these approaches have a number of drawbacks.

Let us consider the shortcomings of the hypothesis of the existence of dark matter. On the one hand, dark matter in both elliptical and spiral galaxies is distributed spherically and symmetrically, that is, regardless of the distribution of visible matter. The spherical distribution of dark matter is proved by the existence of the galaxies NGC 2685, NGC 4650A, A 0136-0801, and ESO 415-G26 (Schweizer et al. 1983) of a gas polar ring located at a distance of three radii of the stellar disk and rotating in a plane perpendicular to the stellar disk. On the other hand, the rotation speed of the ring corresponds to the velocity of the boundary of the stellar disk, which means that the masses of dark and visible matter correlate with each other in a certain way (McGaugh et al. 2016). To date, this contradiction has not been resolved within the framework of the hypothesis of the existence of dark matter.

Secondly, there is the MDAR (Mass Discrepancy-Acceleration Relation) problem, which defines the dominant role in

Received 30 JUN 2022 **Revised** 11 AUG 2022 **Accepted** 21 AUG 2022
†**Corresponding Author**
Tel: +7-926-533-82-10, E-mail: portnovyura@yandex.ru
ORCID: https://orcid.org/0000-0001-6317-687X

http://janss.kr pISSN: 2093-5587 eISSN: 2093-1409

determining accelerations in any galaxies for visible matter. Thus, the study of the movement of 400 stars at distances up to 13,000 light-years from the Sun did not reveal the influence of dark matter (Bidin et al. 2012), from which it could be concluded that there is no dark matter inside the galactic disk. The same conclusion follows from the Tully-Fisher relation (Verheijen 2001), according to which the luminosity of the galaxy, proportional to the mass, ideally correlates with the speed of its rotation. That is, within the framework of the dark matter hypothesis, it remains unclear why the more massive dark matter remains outside the galactic disk and does not collapse into the galactic disk.

Other models include the work (Farnes 2018), in which the authors combine dark matter and dark energy into one phenomenon – an ideal liquid with a negative mass. But this model today has a small calculation base and is also not confirmed experimentally in everything. In (Babourova et al. 2018), the Weyl-Dirac conformal theory of gravity is considered, which is Cartan-Weyl space-time gravitation theory with a Dirac scalar field to model dark matter. However, like in other theories with scalar fields, there remains an essential problem of detecting such scalar fields.

Let us consider the shortcomings of hypotheses about modified theories of gravity. Currently, there are two theories according to which the physical nature of gravity changes on large scales: MoND and TeVeS (Milgrom 2011). MOND cannot explain gravitational lensing, nor can it explain the discrepancy in the calculations of the center of mass of a system of colliding galaxies in their mutual motion and in the radiation of visible matter (Milgrom 2011). The shortcomings of TeVeS include the incapability of simultaneously explaining cosmic microwave background anisotropy and structure formation. It is also shown in (Jain et al. 2013) that some effects predicted by TeVeS are not confirmed within the accuracy of measurements. In addition, both MoND and TeVeS theories cannot explain the absence of the dark matter effect in two ultradiffusive galaxies (Cohen et al. 2018; van Dokkum et al. 2018).

These problems identified in the main hypotheses need to be addressed.

2. METHODS

In Newtonian mechanics, equations describing translational and rotational motion are similar in their form. This evokes the notion of a certain symmetry between translational and rotational motion. However the theory of relativity disrupts this symmetry. So in the theory of relativity, inertial translational motion is determined by a geodesic plotted in four-dimensional space-time, while the inertial rotational movement uses a vector of angular velocity which only moves along the geodesic. Our past studies (Portnov 2015; Portnov 2018; Portnov 2021) provided arguments for restoring the symmetry between translational and rotational motion. To that end in (Portnov 2015; Portnov 2018; Portnov 2021) we introduced the concept of a seven-dimensional phase space-time where inertial translational and rotational movement would be represented by a curve that is the geodesic for the metric of the particular phase space-time. Thus the equations for translational and rotational movement alike are determined by the principle of least action. However, if curved phase space-time is considered, complete symmetry between translational and rotational motion could not be attained. The next step toward achieving symmetry between translational and rotational motion was taken in (Portnov 2022). It is known that inert mass used in translational motion has an equivalent gravitational mass. So it was hypothesized in (Portnov 2022) that the moment of inertia as a measure of inertia in rotational motion would similarly have a corresponding equivalent gravitational moment of inertia. With that in mind, the force of gravitational interaction with a point mass m is determined by the equation:

$$F = \frac{GMm}{R^2} + \frac{DJm}{R^3} \tag{1}$$

where M and J are the gravitational mass and moment of inertia of the body that generates the gravitational field, G is Newton's gravitational constant; D is some new constant of interaction, R is a distance from the body that generates the gravitational field to the point mass m. Using Eq. (1), we obtain the equation of the orbital velocity of the point mass for stable orbital motion:

$$v = \sqrt{\frac{GM}{R} + \frac{DJ}{R^2}}\,. \tag{2}$$

It should be noted that visible matter exists beyond the boundaries of the galactic disc. It is comprised by accumulated gases such as atomic hydrogen HI and molecular hydrogen H_2 whose presence can be detected in the X-ray band (Thean et al. 1997; Battaglia et al. 2006; Vikhlinin et al. 2006). But the surface luminosity of gas, and hence its mass, is not enough to account for the velocities of gas and star motion outside of the stellar disc. Yet the gas, due to its extensive dimensions, has a significant moment

of inertia which, according to Eq. (1), can influence motion velocities of test bodies in an essential manner. In support of the hypothesis positing the existence of a gravitational moment of inertia, velocity curves are computed in (Portnov 2022) for three spiral galaxies. It is shown that the use of Eq. (2) for the computation of galaxy velocity curves agrees well with observed values. There is a number of weak points in (Portnov 2022) as rotation velocities are validated over a rather narrow sample in galaxies and a multitude of parameters are left free. To illustrate, six free parameters were introduced for simulating the density of a galaxy's stellar disc and gas densities. Five parameters would be necessary to bring the model of mass distribution in a galaxy into alignment with observed data on the latter's luminosity. Another free parameter was the interaction constant D.

3. RESULTS

In this study we will test our hypothesis by computing rotation velocity curves for fourteen galaxies as we reduce the number of the parameters. With that goal in mind, our method for computing moments of inertia relies on a known distribution of masses of the stellar bulge, the stellar disc and gas. Table 1 summarizes the parameters of galaxies in the sample.

The distribution of mass in the bulge of the galaxy $M_b(R)$, in the disk of the galaxy $M_d(R)$ and gas $M_g(R)$ is taken from (Begeman 1989; Corbelli & Salucci 2000; Freese 2009; Doroshkevich et al. 2012; Haghi et al. 2016). Using the gas mass distribution, we calculate the gas density distribution:

$$\rho_g(R) = \frac{dM_g}{dV}.$$

The distribution of the moment of inertia for the stellar bulge and the disk was found by splitting the stellar bulge and the disk into $2\Delta R$ thick layers with the moments of inertia:

$$\Delta J_{b+d}(R_k) = \alpha R_k^{\,2} \sum_i m_i\Big|_{R_k-\Delta R\le R_i\le R_k+\Delta R},$$

where m_i, R_i is the mass and distance from the center of the galaxy of the i star, R_k is the distance from the center of the galaxy to the middle of the $2\Delta R$ thick layer, α is some constant reflecting the distribution of stars in the galactic disk. Note that in this equation, the masses of only such stars are considered, the distances R_i to which lie in the interval $R_k - \Delta R \le R_i \le R_k + \Delta R$. Then, the total moment of inertia of the stellar bulge and the disk with radius R is found as:

$$J_{b+d}(R) = \sum_k \Delta J_{b+d}(R_k)\Big|_{R_k\le R}.$$

The moment of inertia for gas due to its spherically symmetric distribution around the galaxy will be sought as an integral over all moments of inertia of spherical layers $dJ_g(r) = \frac{2}{3} r^2 dm_g$:

$$J_g(R) = \int_0^R \left(\frac{8}{3}\pi\rho_g(r) r^4\right) dr.$$

Table 1. Parameters of galaxies

Name of galaxy	Distance (Mpc)	Morphological type	Optical center (α, δ J2000)		Visual diameter (arcmin)
NGC 6503	5.272 ± 0.589	Sc	$17^h49^m36.56^s$	+70°08'39.6''	7.1
NGC 0598	0.847 ± 0.024	Sc	$01^h33^m50.91^s$	+30°39'35.5''	69.2
NGC 3198	14.488 ± 0.406	Sc	$10^h19^m54.93^s$	+45°32'59.2''	3.0
NGC 4789A	4.036 ± 0.066	Ir	$12^h54^m05.47^s$	+27°09'02.1''	2.5
NGC 3521	13.804 ± 3.897	Sbc	$11^h05^m48.76^s$	–00°02'04.9''	13.5
NGC 3621	6.516 ± 0.276	Sd	$11^h18^m16.49^s$	–32°48'50.3''	12.40
NGC 5055	9.036 ± 0.084	Sbc	$13^h15^m49.31^s$	+42°01'45.6''	3.3
NGC 2998	58.345 ± 13.435	Sc	$09^h48^m43.63^s$	+44°04'53.2''	2.6
NGC 4100	20.045 ± 4.616	Sbc	$12^h06^m08.57^s$	+49°34'58.2''	5.6
NGC 4183	17.219 ± 3.965	Scd	$12^h13^m16.90^s$	+43°41'54.8''	5.5
NGC 5033	19.055 ± 4.388	Sc	$13^h13^m27.52^s$	+36°35'37.8''	1.82
NGC 5371	32.659 ± 5.889	Sbc	$13^h55^m39.95^s$	+40°27'42.3''	4.5
NGC 5533	46.345 ± 10.672	Sb	$14^h16^m07.74^s$	+35°20'37.7''	3.7
NGC 3769	16.293 ± 2.938	Sb	$11^h37^m44.11^s$	+47°53'35.5''	3.3

Adapted from Makarov (2014) with permission of EDP Sciences.

In this paper, the integral of the moment of inertia of gas will be found by the method of Riemann sum. Then, using Eq. (2), we find the orbital velocity of the point mass:

$$V=\sqrt{\frac{G\left(M_b+M_d+M_g\right)}{R}+\frac{D\left(J_{b+d}+J_g\right)}{R^2}}.$$

In the numerical simulation of velocities, two free parameters D and α were selected in this way (Table 2) so that the obtained velocity value coincides with the observed values (Begeman 1989; Corbelli & Salucci 2000; Freese 2009; Doroshkevich et al. 2012; Haghi et al. 2016). It is interesting to note here that the parameter α = 1 was obtained for an irregular galaxy, while for spiral galaxies it is less than one. The calculated velocities for galaxies are summarized in Tables 3–16. The graphs in Figs. 1–3 show the observational velocity curves (Begeman 1989; Corbelli & Salucci 2000; Freese 2009; Doroshkevich et al. 2012; Haghi et al. 2016) and the velocity curves calculated in the model under discussion (Tables 3–16).

As can be seen from Tables 3–16, inside the galactic disk, the moment of inertia of gas J_g and the moment of inertia of the disk J_d or bulge + disk J_{b+d} are very small, this explains the fact that there is no noticeable deviation of the stellar movement dynamics from the distribution of the mass of visible matter inside the galactic disk. Outside the galactic disk, the moment of inertia of gas J_g begins to increase sharply, therefore, the term with the moment of inertia begins to prevail in Eq. (1); this fact circumstance explains why the motion dynamics of test bodies outside the galactic disk differs from the distribution of the mass of visible matter.

As can be seen from the graphs shown in Figs. 1–3, the velocity curves obtained based on the calculations of the model under discussion are comparable in order of magnitude with the observed velocity curves of the rotation of galaxies. The existing discrepancies between the model curve and the observation curve can be caused by errors accumulated during numerical modeling and errors in determining the volume densities of gas. Note that such a coincidence is obtained with no dark matter involved. In this case, the magnitude of the interaction constant D for all galaxies coincides in order of magnitude (Table 2).

Table 2. Selected model parameters

Name of galaxy	α	$D\times10^{-30}$ (N·m/kg^2)	Name of galaxy	α	$D\times10^{-30}$ (N·m/kg^2)
NGC 6503	0.20	6.0	NGC 2998	0.10	1.5
NGC 0598	0.15	6.0	NGC 4100	0.01	6.5
NGC 3198	0.04	2.4	NGC 4183	0.25	2.5
NGC 4789A	1.00	6.4	NGC 5033	0.03	2.3
NGC 3521	0.03	1.5	NGC 5371	0.03	2.0
NGC 3621	0.10	3.0	NGC 5533	0.02	2.1
NGC 5055	0.03	1.8	NGC 3769	0.01	4.5

Table 3. Rotation curve of NGC 6503

r (kpc)	$J_d\times10^{79}$ (kg·m^2)	$J_g\times10^{79}$ (kg·m^2)	V (km/s)	r (kpc)	$J_d\times10^{79}$ (kg·m^2)	$J_g\times10^{79}$ (kg·m^2)	V (km/s)	r (kpc)	$J_d\times10^{79}$ (kg·m^2)	$J_g\times10^{79}$ (kg·m^2)	V (km/s)
1	0.06	0.001	106	8	1.92	5.08	108	15	2.02	38.5	120
2	0.41	0.025	128	9	1.94	7.92	110	16	2.03	43.0	118
3	0.93	0.115	129	10	1.96	11.6	112	17	2.04	47.4	116
4	1.32	0.339	120	11	1.98	16.3	115	18	2.05	50.1	113
5	1.77	0.798	116	12	1.99	21.8	118	19	2.05	52.6	110
6	1.85	1.66	110	13	2.01	27.7	120	20	2.06	54.8	106
7	1.89	3.05	108	14	2.02	33.2	120	21	2.06	63.7	108

Table 4. Rotation curve of NGC 598

r (kpc)	$J_d\times10^{79}$ (kg·m^2)	$J_g\times10^{79}$ (kg·m^2)	V (km/s)	r (kpc)	$J_d\times10^{79}$ (kg·m^2)	$J_g\times10^{79}$ (kg·m^2)	V (km/s)	r (kpc)	$J_d\times10^{79}$ (kg·m^2)	$J_g\times10^{79}$ (kg·m^2)	V (km/s)
1	0.01	0.003	57	6	0.69	3.98	111	11	0.74	20.3	118
2	0.10	0.061	82	7	0.72	6.94	117	12	0.74	22.1	112
3	0.28	0.282	94	8	0.72	10.8	123	13	0.74	23.2	107
4	0.43	0.843	98	9	0.73	14.9	124	14	0.74	24.8	103
5	0.59	1.98	104	10	0.73	18.4	123	15	0.74	25.5	98

Table 5. Rotation curve of NGC 3198

r (kpc)	$J_d \times 10^{79}$ (kg·m^2)	$J_g \times 10^{79}$ (kg·m^2)	V (km/s)	r (kpc)	$J_d \times 10^{79}$ (kg·m^2)	$J_g \times 10^{79}$ (kg·m^2)	V (km/s)	r (kpc)	$J_d \times 10^{79}$ (kg·m^2)	$J_g \times 10^{79}$ (kg·m^2)	V (km/s)
0	0.00	0.00	0	15	8.88	72.5	147	30	9.23	514	148
5	2.06	0.57	152	20	9.05	189	150	35	9.29	554	134
10	6.11	21.7	154	25	9.16	366	153	40	9.33	586	122

Table 6. Rotation curve of NGC 4789A

r (kpc)	$J_d \times 10^{79}$ (kg·m^2)	$J_g \times 10^{79}$ (kg·m^2)	V (km/s)	r (kpc)	$J_d \times 10^{79}$ (kg·m^2)	$J_g \times 10^{79}$ (kg·m^2)	V (km/s)	r (kpc)	$J_d \times 10^{79}$ (kg·m^2)	$J_g \times 10^{79}$ (kg·m^2)	V (km/s)
0	0.000	0.000	0	3	0.020	0.116	37	6	0.459	0.999	49
1	0.001	0.002	16	4	0.045	0.321	44	7	0.046	1.450	50
2	0.008	0.032	30	5	0.046	0.620	47	8	0.046	1.849	49

Table 7. Rotation curve of NGC 3521

r (kpc)	$J_d \times 10^{79}$ (kg·m^2)	$J_g \times 10^{79}$ (kg·m^2)	V (km/s)	r (kpc)	$J_d \times 10^{79}$ (kg·m^2)	$J_g \times 10^{79}$ (kg·m^2)	V (km/s)	r (kpc)	$J_d \times 10^{79}$ (kg·m^2)	$J_g \times 10^{79}$ (kg·m^2)	V (km/s)
2	0.17	0.00	162	12	14.8	70.8	219	22	17.9	549	207
4	1.72	0.00	214	14	17.5	135	218	24	18.0	601	198
6	5.25	2.33	233	16	17.6	233	218	26	18.0	642	190
8	9.16	12.0	233	18	17.8	347	216	28	18.1	691	183
10	12.1	32.6	224	20	17.9	471	214	30	18.1	758	178

Table 8. Rotation curve of NGC 3621

r (kpc)	$J_d \times 10^{79}$ (kg·m^2)	$J_g \times 10^{79}$ (kg·m^2)	V (km/s)	r (kpc)	$J_d \times 10^{79}$ (kg·m^2)	$J_g \times 10^{79}$ (kg·m^2)	V (km/s)	r (kpc)	$J_d \times 10^{79}$ (kg·m^2)	$J_g \times 10^{79}$ (kg·m^2)	V (km/s)
2	0.16	0.00	88	10	7.78	23.0	140	18	10.4	111	141
4	1.61	0.50	128	12	9.67	36.9	138	20	10.5	141	141
6	3.55	3.53	136	14	10.3	57.4	139	22	10.5	163	136
8	5.53	11.7	140	16	10.4	81.7	139	24	10.6	178	130

Table 9. Rotation curve of NGC 5055

r (kpc)	$J_{b+d} \times 10^{79}$ (kg·m^2)	$J_g \times 10^{79}$ (kg·m^2)	V (km/s)	r (kpc)	$J_{b+d} \times 10^{79}$ (kg·m^2)	$J_g \times 10^{79}$ (kg·m^2)	V (km/s)	r (kpc)	$J_{b+d} \times 10^{79}$ (kg·m^2)	$J_g \times 10^{79}$ (kg·m^2)	V (km/s)
2.5	0.67	0.00	186	17.5	36.2	302	220	32.5	38.4	691	168
5.0	3.46	0.00	198	20.0	36.7	403	212	35.0	38.6	777	164
7.5	8.75	5.28	205	22.5	37.2	476	201	37.5	38.8	856	159
10.0	16.3	24.6	209	25.0	37.6	535	191	40.0	38.9	1,039	159
12.5	21.8	73.3	208	27.5	37.9	579	181	42.5	39.0	1,424	165
15.0	26.5	172	213	30.0	38.2	627	173	45.0	39.2	1,883	171

Table 10. Rotation curve of NGC 2998

r (kpc)	$J_{b+d} \times 10^{79}$ (kg·m^2)	$J_g \times 10^{79}$ (kg·m^2)	V (km/s)	r (kpc)	$J_{b+d} \times 10^{79}$ (kg·m^2)	$J_g \times 10^{79}$ (kg·m^2)	V (km/s)	r (kpc)	$J_{b+d} \times 10^{79}$ (kg·m^2)	$J_g \times 10^{79}$ (kg·m^2)	V (km/s)
3	2.24	0.031	204	18	123	183	207	33	129	2,143	226
6	10.2	1.00	203	21	126	340	204	36	129	2,745	229
9	25.7	8.27	200	24	127	583	204	39	129	3,212	226
12	51.3	32.8	201	27	128	940	209	42	130	3,581	220
15	85.3	86.1	204	30	129	1,460	217	45	130	3,905	214

Table 11. Rotation curve of NGC 4100

r (kpc)	$J_d \times 10^{79}$ (kg·m^2)	$J_g \times 10^{79}$ (kg·m^2)	V (km/s)	r (kpc)	$J_d \times 10^{79}$ (kg·m^2)	$J_g \times 10^{79}$ (kg·m^2)	V (km/s)	r (kpc)	$J_d \times 10^{79}$ (kg·m^2)	$J_g \times 10^{79}$ (kg·m^2)	V (km/s)
1	0.001	0.000	36	7	1.68	3.42	202	13	1.82	27.0	175
2	0.046	0.007	135	8	1.74	5.25	193	14	1.83	33.6	174
3	0.121	0.062	146	9	1.77	7.78	186	15	1.84	39.5	172
4	0.338	0.277	169	10	1.78	11.2	181	16	1.85	42.8	167
5	0.800	0.867	193	11	1.80	15.5	179	17	1.85	44.5	161
6	1.36	2.06	206	12	1.81	20.9	177	18	1.86	45.6	155

Table 12. Rotation curve of NGC 4183

r (kpc)	$J_d \times 10^{79}$ (kg·m^2)	$J_g \times 10^{79}$ (kg·m^2)	V (km/s)	r (kpc)	$J_d \times 10^{79}$ (kg·m^2)	$J_g \times 10^{79}$ (kg·m^2)	V (km/s)	r (kpc)	$J_d \times 10^{79}$ (kg·m^2)	$J_g \times 10^{79}$ (kg·m^2)	V (km/s)
1	0.021	0.000	50	7	6.48	7.12	116	13	9.48	57.5	122
2	0.189	0.020	69	8	7.96	11.8	119	14	9.53	62.5	118
3	0.632	0.144	81	9	8.78	18.5	121	15	9.57	65.6	113
4	1.38	0.575	90	10	9.28	27.3	123	16	9.61	68.2	108
5	2.57	1.61	99	11	9.36	37.4	124	17	9.64	69.6	103
6	4.19	3.65	107	12	9.43	47.7	123	18	9.67	70.1	99

Table 13. Rotation curve of NGC 5033

r (kpc)	$J_d \times 10^{79}$ (kg·m^2)	$J_g \times 10^{79}$ (kg·m^2)	V (km/s)	r (kpc)	$J_d \times 10^{79}$ (kg·m^2)	$J_g \times 10^{79}$ (kg·m^2)	V (km/s)	r (kpc)	$J_d \times 10^{79}$ (kg·m^2)	$J_g \times 10^{79}$ (kg·m^2)	V (km/s)
0	0.000	0.000	0	7	3.78	4.09	211	19	49.9	233	224
1	0.058	0.001	213	9	8.15	10.6	210	22	50.3	390	221
2	0.330	0.016	236	11	11.9	24.0	207	25	50.6	568	219
3	0.893	0.109	243	13	16.6	49.1	206	28	50.8	704	211
4	1.69	0.420	241	15	22.7	91.1	209	31	50.9	750	198
5	2.43	1.18	231	17	34.3	152	216	34	51.1	768	186

Table 14. Rotation curve of NGC 5371

r (kpc)	$J_{b+d} \times 10^{79}$ (kg·m^2)	$J_g \times 10^{79}$ (kg·m^2)	V (km/s)	r (kpc)	$J_{b+d} \times 10^{79}$ (kg·m^2)	$J_g \times 10^{79}$ (kg·m^2)	V (km/s)	r (kpc)	$J_{b+d} \times 10^{79}$ (kg·m^2)	$J_g \times 10^{79}$ (kg·m^2)	V (km/s)
1	0.060	0.000	217	8	6.37	0.015	208	21	70.6	522	251
2	0.333	0.000	237	10	14.6	2.84	216	24	71.0	632	238
3	0.914	0.000	244	12	20.3	25.4	216	27	71.3	729	225
4	1.59	0.000	236	14	27.2	88.9	224	30	71.6	773	211
5	2.24	0.000	223	16	43.5	211	244	33	71.8	794	198
6	3.37	0.000	218	18	60.4	355	256	36	71.9	811	187

Table 15. Rotation curve of NGC 5533

r (kpc)	$J_{b+d} \times 10^{79}$ (kg·m^2)	$J_g \times 10^{79}$ (kg·m^2)	V (km/s)	r (kpc)	$J_{b+d} \times 10^{79}$ (kg·m^2)	$J_g \times 10^{79}$ (kg·m^2)	V (km/s)	r (kpc)	$J_{b+d} \times 10^{79}$ (kg·m^2)	$J_g \times 10^{79}$ (kg·m^2)	V (km/s)
0	0.00	0.000	0	25	67.0	593	250	50	114	5,504	267
5	10.7	0.049	327	30	74.8	1,168	253	55	115	7,034	269
10	38.5	8.50	309	35	77.2	1,870	253	60	116	7,741	258
15	52.3	57.6	269	40	88.2	2,771	255	65	116	8,175	246
20	59.6	219	250	45	100	4,038	262	70	117	8,653	236

Summarizing the found interaction constants D for all galaxies (Table 2), we find the average interaction constant:

$$D = (3.4 \pm 1.9) \times 10^{-30}\ \mathrm{N{\cdot}m/kg^2}.$$

Despite the fact that the methods for calculating the velocities in this paper and in (Portnov 2022) are different, the obtained values of the interaction constants D are the same in both papers.

Table 16. Rotation curve of NGC 3769

r (kpc)	$J_d \times 10^{79}$ (kg·m^2)	$J_g \times 10^{79}$ (kg·m^2)	V (km/s)	r (kpc)	$J_d \times 10^{79}$ (kg·m^2)	$J_g \times 10^{79}$ (kg·m^2)	V (km/s)	r (kpc)	$J_d \times 10^{79}$ (kg·m^2)	$J_g \times 10^{79}$ (kg·m^2)	V (km/s)
2	0.030	0.069	99	12	0.306	23.8	112	22	0.325	124	123
4	0.147	1.23	118	14	0.312	41.5	120	24	0.327	160	126
6	0.204	5.49	123	16	0.317	58.7	121	26	0.330	201	130
8	0.286	11.9	125	18	0.321	69.1	117	28	0.331	209	123
10	0.297	17.3	117	20	0.321	94.0	120	30	0.335	212	116

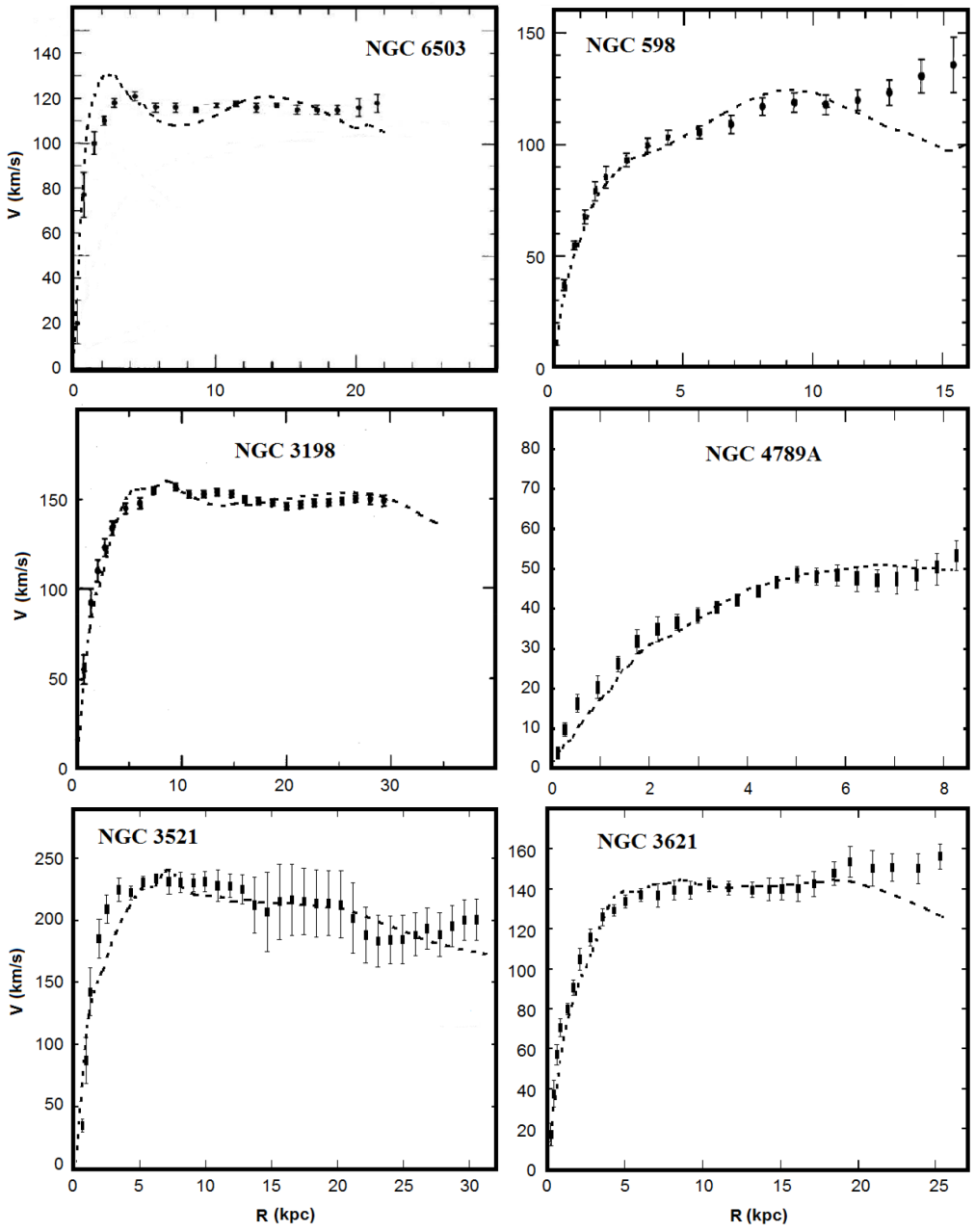

Fig. 1. The rotation curves of galaxies NGC 6503, NGC 598, NGC 3198, NGC 4789A, NGC 3521 and NGC 3621. Error bars show observed rotation velocities of galaxies. Dashed line show velocities plotted using our model discussed in the paper. Adapted from Doroshkevich et al. (2012) with permission of IOP Publishing; Freese (2009) with permission of EDP Sciences; Corbelli & Salucci (2000) with permission of Monthly Notices of the Royal Astronomical Society; Begeman (1989) with permission of EDP Sciences; Haghi et al. (2016) with permission of Monthly Notices of the Royal Astronomical Society.

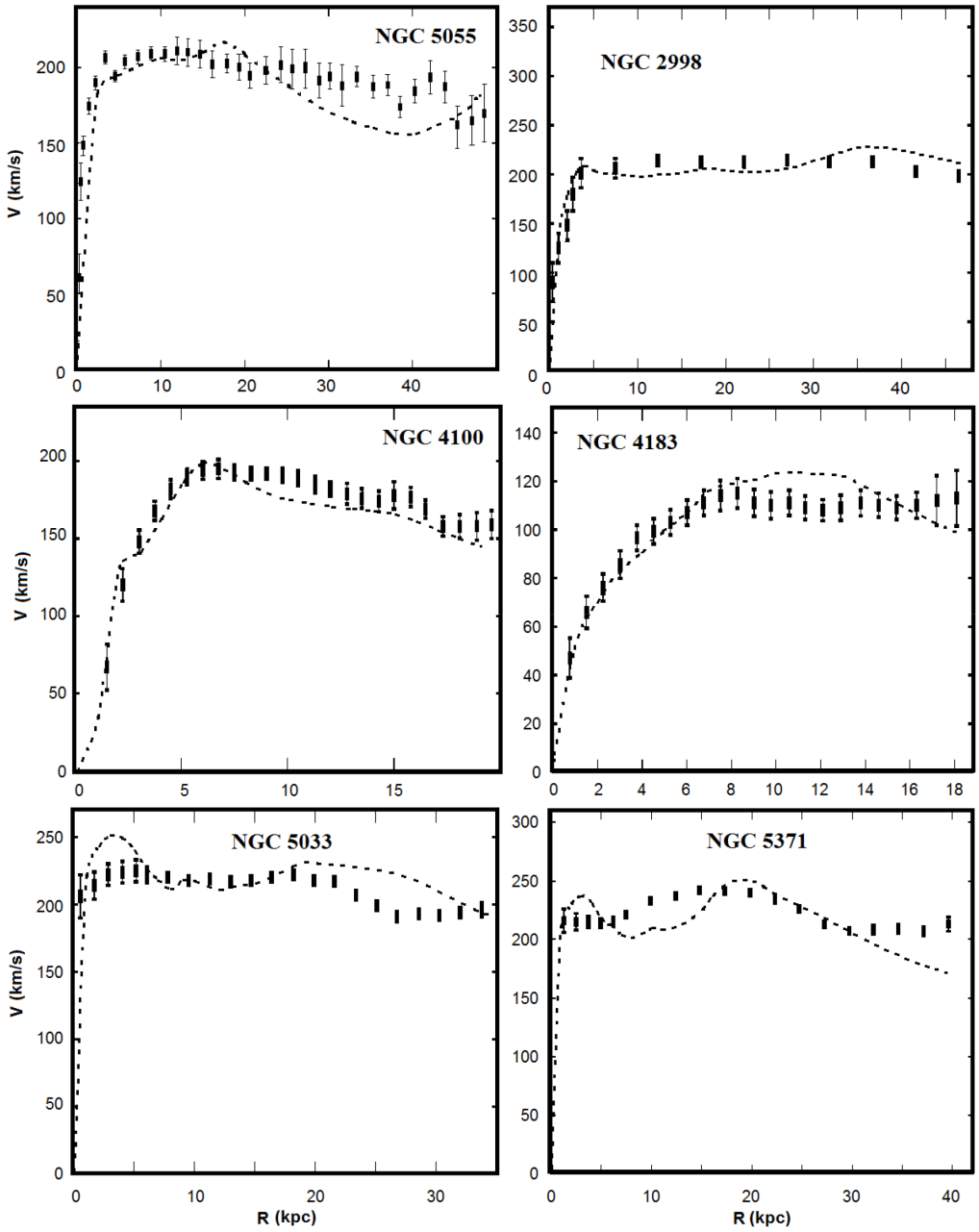

Fig. 2. The rotation curves of galaxies NGC 5055, NGC 2998, NGC 4100, NGC 4183, NGC 5033 and NGC 5371. Error bars show observed rotation velocities of galaxies. Dashed line show velocities plotted using our model discussed in the paper. Adapted from Haghi et al. (2016) with permission of Monthly Notices of the Royal Astronomical Society.

Due to the small value of the interaction constant D and the peculiarity of Eq. (1), on the scale of the solar system for point bodies (the Sun, planets, and small bodies), the contribution of the moment of inertia J due to gravitational interaction will be insignificant, compared to the mass contribution M.

On the galactic scale, the moment of inertia for gas extended in space will be large, so the contribution of the moment of inertia due to the gravitational interaction Eq. (1) becomes predominant, which manifests itself in a higher motion velocity of test bodies outside the galaxy than can be expected from the mass alone.

Separately, we note that due to the influence of the moment of inertia on the gravitational interaction force, the center of mass, determined by the gravitational field of the galaxy, and the center of mass, determined by the apparent

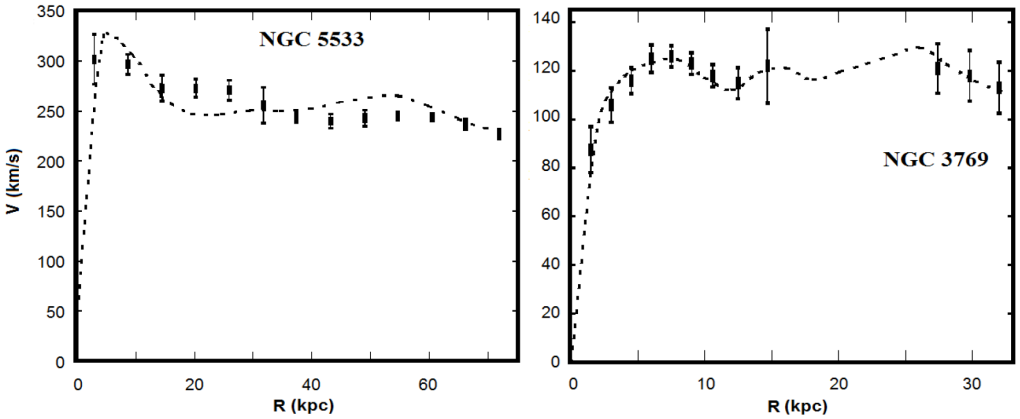

Fig. 3. The rotation curves of galaxies NGC 5533 and NGC 3769. Error bars show observed rotation velocities of galaxies. Dashed line show velocities plotted using our model discussed in the paper. Adapted from Haghi et al. (2016) with permission of Monthly Notices of the Royal Astronomical Society.

distribution of mass in the galaxy, may not coincide. A similar situation may arise when galaxies collide, due to the redistribution of gas around colliding galaxies, the moment of inertia will change, and the gravitational center of mass determined by it will change, too. This may explain why the gravitational center of mass of colliding galaxies does not coincide with the center of mass determined by the distribution of visible matter. The model described herein can be verified by comparing the coordinates of the center of mass of colliding galaxies, calculated from the distribution of gas and from the motion dynamics of the galaxies.

4. CONCLUSION

Summing up, we note that the article has being studied a model to explain the rotation curves of galaxies without involving dark matter. The force created only by the mass of luminous matter cannot explain the shape of the rotation velocity curve. But if we assume that the moment of inertia of gas outside the galaxies also creates a gravitational field, then the rotation curve of the galaxies can be easily explained. At the same time, as shown in the paper, shapes of the observed and modelled rotation curves correlate in order of magnitude. It is also shown that the moment of inertia of gas inside the stellar disk is too small to significantly affect the rotational dynamics of the test bodies, which explains why the rotational dynamics of stars inside the galactic disk is completely explained by the stellar mass.

Using numerical simulation based on data from fourteen galaxies, the constant of gravitational interaction caused by the moment of inertia was found D. The very small value of the constant D makes it possible to explain the absence of the moment of inertia influence on the gravitational interaction on the scale of the solar system.

In addition, the hypothesis under discussion about the influence of the moment of inertia of a weakly massive, but spatially extended gas on the gravitational potential of the galaxy can explain the lack of coincidence of the center of mass of colliding galaxies, calculated from the distribution of stars and the dynamic motion of the galaxies themselves.

We also pay attention to two ultradiffusive galaxies NGC 1052-DF2 and NGC1052-DF4, in which there is a very little or completely no dark matter (Cohen et al. 2018; van Dokkum et al. 2018). As follows from the proposed model, the rotation curves of galaxies are explained by the moment of inertia created by gas. Therefore, for ultradiffusive galaxies, which have no gas outside the stellar disk, there is no moment of inertia, which could create an additional gravitational field. That is, the being studied a model naturally explains the absence of dark matter for ultradiffusive galaxies, which is not possible in the theories of MoND and TeVeS.

The study of ultradiffusive galaxies and the comparison of their rotation curves with those in galaxies with a high content of gas lying outside the galactic disks will allow for concluding that the proposed model is reliable.

ACKNOWLEDGMENTS

I am very grateful to my wife and daughter, who supported me for several months while I was working on the article.

ORCID

Yuriy A. Portnov https://orcid.org/0000-0001-6317-687X

REFERENCES

Babourova OV, Frolov BN, Kudlaev PE, Axially symmetric solution of the Weyl-Dirac theory of gravitation and the problem of rotation curves of galaxies, Gravit. Cosmol. 24, 118-121 (2018). https://doi.org/10.1134/S0202289318020020

Battaglia G, Fraternali F, Oosterloo T, Sancisi R, Hi study of the warped spiral galaxy NGC5055: a disk/dark matter halo offset? Astron. Astrophys. 447, 49-62 (2006). https://doi.org/10.1051/0004-6361:20053210

Begeman KG, H I rotation curves of spiral galaxies: I - NGC 3198, Astron. Astrophys. 223, 47-60 (1989).

Bidin CM, Carraro G, Méndez RA, Smith R, Kinematical and chemical vertical structure of the Galactic thick disk. II. a lack of dark matter in the solar neighborhood, Astrophys. J. 751, 30 (2012). https://doi.org/10.1088/0004-637X/751/1/30

Cohen Y, van Dokkum P, Danieli S, Romanowsky AJ, Abraham R, et al., The dragonfly nearby galaxies survey. V. HST/ACS observations of 23 low surface brightness objects in the fields of NGC 1052, NGC 1084, M96, and NGC 4258, Astrophys. J. 868, 96 (2018). https://doi.org/10.3847/1538-4357/aae7c8

Corbelli E, Salucci P, The extended rotation curve and the dark matter halo of M33, Mon. Not. R. Astron. Soc. 311, 441-447 (2000). https://doi.org/10.1046/j.1365-8711.2000.03075.x

Doroshkevich AG, Lukash VN, Mikheeva EV, A solution to the problems of cusps and rotation curves in dark matter halos in the cosmological standard model, Phys. Usp. 55, 3 (2012). https://doi.org/10.3367/UFNr.0182.201201a.0003

Farnes JS, A unifying theory of dark energy and dark matter: negative masses and matter creation within a modified ΛCDM framework, Astron. Astrophys. 620, A92 (2018). https://doi.org/10.1051/0004-6361/201832898

Freese K, Review of observational evidence for dark matter in the universe and in upcoming searches for dark stars, EAS Publications Series 36, 113-126 (2009). https://doi.org/10.1051/eas/0936016

Haghi H, Bazkiaei AE, Zonoozi AH, Roupa P, Declining rotation curves of galaxies as a test of gravitational theory, Mon. Not. R. Astron. Soc. 458, 4172-4187 (2016). https://doi.org/10.1093/mnras/stw573

Jain B, Vikram V, Sakstein J, Astrophysical tests of modified gravity: constraints from distance indicators in the nearby universe, Astrophys. J. 779, 39 (2013). https://doi.org/10.1088/0004-637X/779/1/39

Makarov D, Prugniel P, Terekhova N, Courtois, H, Vauglin I, HyperLEDA. III. the catalogue of extragalactic distances, Astron. Astrophys. 570, A13 (2014). https://doi.org/10.1051/0004-6361/201423496

McGaugh SS, Lelli F, Schombert JM, The radial acceleration relation in rotationally supported galaxies, Phys. Rev. Lett. 117, 201101 (2016). https://doi.org/10.1103/PhysRevLett.117.201101

Milgrom M, MD or DM? Modified dynamics at low accelerations vs dark matter, Pos. Proc. Sci. 109, 033 (2011). https://doi.org/10.22323/1.109.0033

Portnov YA, Formation of the initial distribution of matter inhomogeneities in the era of radiation domination, Int. J. Geom. Methods Mod. Phys. 12, 1550097 (2015). https://doi.org/10.1142/S0219887815500978

Portnov YA, Moment of inertia of gas as a source of added gravitational field in galaxies, J. Astron. Space Sci. 39, 59-65 (2022). https://doi.org/10.5140/JASS.2022.39.2.59

Portnov YA, On the invariance in the inhomogeneous Lorentz group SO(1,3) in the context of optical vortex description, Gen. Relativ. Gravit. 53, 11 (2021). https://doi.org/10.1007/s10714-021-02788-1

Portnov YA, The gravitational redshift of a optical vortex being different from that of an gravitational redshift plane of an electromagnetic wave, J. Astrophys. Astron. 39, 38 (2018). https://doi.org/10.1007/s12036-018-9530-9

Schweizer F, Whitmore BC, Rubin VC, Colliding and merging galaxies. II - SO galaxies with polar rings, Astron. J. 88, 909-925 (1983). https://doi.org/10.1086/113377

Thean AHC, Mundell CG, Pedlar A, Nicholson RA, A neutral hydrogen study of the Seyfert galaxy NGC 5033, Mon. Not. R. Astron. Soc. 290, 15-24 (1997). https://doi.org/10.1093/mnras/290.1.15

van Dokkum P, Danieli S, Cohen Y, Merritt A, Romanowsky AJ, et al., A galaxy lacking dark matter, Nature. 555, 629-632 (2018). https://doi.org/10.1038/nature25767

Verheijen MAW, The ursa major cluster of galaxies. V. H I rotation curve shapes and the tully-fisher relations, Astrophys. J. 563, 694-715 (2001). https://doi.org/10.1086/323887

Vikhlinin A, Kravtsov A, Forman W, Jones C, Markevitch M, et al., *Chandra* sample of nearby relaxed galaxy clusters: mass, gas fraction, and mass–temperature relation, Astrophys. J. 640, 691-709 (2006). https://doi.org/10.1086/500288